

# Rationally Designed Polypharmacology: $\alpha$ -Helix Mimetics as Dual Inhibitors of the Oncoproteins Mcl-1 and HDM2

Ivie L. Conlon,<sup>[a]</sup> Brandon Drennen,<sup>[a]</sup> Maryanna E. Lanning,<sup>[a]</sup> Samuel Hughes,<sup>[b]</sup> Rebecca Rothhaas,<sup>[a]</sup> Paul T. Wilder,<sup>[c]</sup> Alexander D. MacKerell, Jr.,<sup>[a]</sup> and Steven Fletcher\*<sup>[a]</sup>

Protein–protein interactions (PPIs), many of which are dominated by  $\alpha$ -helical recognition domains, play key roles in many essential cellular processes, and the dysregulation of these interactions can cause detrimental effects. For instance, aberrant PPIs involving the Bcl-2 protein family can lead to several diseases including cancer, neurodegenerative diseases, and diabetes. Interactions between Bcl-2 pro-life proteins, such as Mcl-1, and pro-death proteins, such as Bim, regulate the intrinsic pathway of apoptosis. p53, a tumor-suppressor protein, also has a pivotal role in apoptosis and is negatively regulated by its E3 ubiquitin ligase HDM2. Both Mcl-1 and HDM2 are upregulated in numerous cancers, and, interestingly, there is crosstalk between both protein pathways. Recently, synergy has been observed between Mcl-1 and HDM2 inhibitors. Towards the development of new anticancer drugs, we herein describe a polypharmacology approach for the dual inhibition of Mcl-1 and HDM2 by employing three densely functionalized isoxazoles, pyrazoles, and thiazoles as mimetics of key  $\alpha$ -helical domains of their partner proteins.

## Introduction

Protein–protein interactions (PPIs) are involved in crucial cellular pathways including proliferation, differentiation, and apoptosis.<sup>[1,2]</sup> Dysregulations of PPIs cause a host of different diseases, including cancer, neurodegenerative disorders, auto-immunity complications and diabetes.<sup>[1–5]</sup> Typically, PPI interfaces cover large surface areas and consist of flat hydrophobic regions with noncontiguous contact points, rendering drug design challenging.<sup>[6–9]</sup> However, many academic and industrial groups have successfully targeted these interactions with small

molecules, several of which in various stages of clinical trials.<sup>[10–13]</sup> Tools such as alanine scanning mutagenesis have been instrumental in identifying key residues located in “hot spots” that account for a large degree of the energetic stability of the complexes. In  $\alpha$ -helix-mediated PPIs, these “hot spots” often involve the  $i$ ,  $i+3/4$ , and  $i+7$  residues that are oriented on one side of the helix.<sup>[14–16]</sup> The B-cell lymphoma-2 (Bcl-2) family and human double minute 2 (HDM2) engage in such  $\alpha$ -helix-mediated PPIs and their aberrant regulations are directly associated with tumorigenesis.<sup>[17,18]</sup>

The Bcl-2 family of proteins are key regulators of cell life and death, and constitute the intrinsic pathway of apoptosis.<sup>[17,19]</sup> The family comprises three subgroups: the anti-apoptotic proteins myeloid cell leukemia-1 (Mcl-1), Bcl-2, Bcl-xL, Bcl-w and Bfl-1; multidomain pro-apoptotic proteins Bak and Bax; and BH3-only pro-apoptotic proteins including Bim, Bid, PUMA, and NOXA. When the cell receives apoptotic stimuli due to different stressors such as DNA damage or growth-factor deprivation, BH3-only proteins are upregulated and, through their  $\alpha$ -helical BH3 “death” domains (Figure 1A), bind the anti-apoptotic proteins to release Bak and Bax, leading to homodimerization of these proteins.<sup>[17,19]</sup> In turn, this leads to mitochondrial outer-membrane permeabilization (MOMP), ultimately allowing the release of apoptosis-inducing proteins such as cytochrome *c*.<sup>[17,19]</sup> During the formation of malignancies dependent on Bcl-2 proteins, the anti-apoptotic proteins are overexpressed and the BH3-only proteins are unable to compensate, causing cell immortality.<sup>[17–20]</sup>

HDM2 is an E3 ubiquitin protein ligase responsible for the degradation of the tumor-suppressor protein p53 through binding its  $\alpha$ -helical transactivation domain (TAD; Figure 1C).<sup>[21,22]</sup> p53 is a short-lived protein whose concentration at any given time is controlled by the rate at which it is degraded.<sup>[23]</sup> It is coined the “guardian of the genome” due to its involvement in a variety of cellular pathways, notably the transcription of genes during cell stress events involved in apoptosis, DNA repair, senescence, and metabolic homeostasis. In turn it is negatively regulated by HDM2.<sup>[22,24]</sup> During tumorigenesis, HDM2 can be overexpressed, thus inhibiting the activation of p53 and decreasing cell death.<sup>[25]</sup> p53 regulates apoptosis with both the transcription-dependent and -independent pathways, crossing paths with Bcl-2 proteins.<sup>[23]</sup> Within the transcription-dependent pathway, it transcribes genes necessary for cell senescence and apoptosis such as p21 and the BH3-only protein PUMA.<sup>[18]</sup> Importantly, this pathway involves the translocation of p53 from the nucleus to the mitochondria, allowing interactions with various members of

[a] I. L. Conlon, Dr. B. Drennen, Dr. M. E. Lanning, R. Rothhaas, Dr. A. D. MacKerell, Jr., Dr. S. Fletcher  
Department of Pharmaceutical Sciences  
University of Maryland School of Pharmacy  
Baltimore, MD 21201 (USA)  
E-mail: steven.fletcher@rx.umaryland.edu

[b] S. Hughes  
School of Chemistry, Cardiff University  
Cardiff, CF10 3AT (UK)

[c] Dr. P. T. Wilder  
Department of Biochemistry and Molecular Biology  
Center for Biomolecular Therapeutics  
University of Maryland School of Medicine  
Baltimore, MD 21201 (USA)

 Supporting information for this article is available on the WWW under <https://doi.org/10.1002/cmdc.202000278>

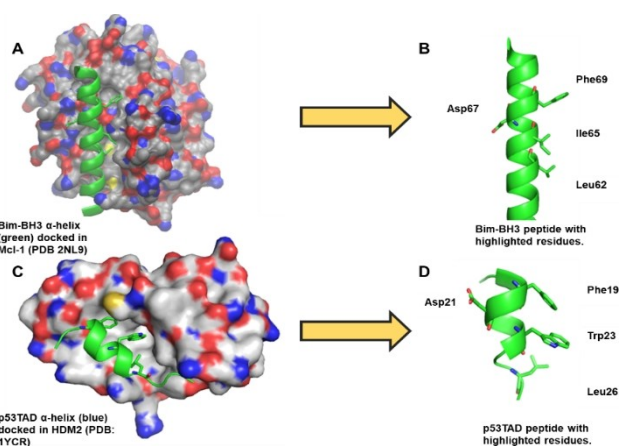


**Figure 1.** A) Co-crystal structure of Bim-BH3 bound to Mcl-1 (PDB ID: 2NL9). B) Hot spot residues highlighted in Bim-BH3 peptide. C) Co-crystal structure of p53TAD bound to HDM2 (PDB ID: 1YCR). D) Hot spot residues highlighted in p53TAD.

the Bcl-2 family.<sup>[26]</sup> p53 can bind anti-apoptotic proteins directly or disrupt pro- and anti-apoptotic interactions such as the Bak/Mcl-1.<sup>[27]</sup> Additionally, it can directly bind Bax, which can then translocate and homodimerize on the mitochondrial outer membrane, leading to MOMP.<sup>[17,23,27–29]</sup> Together these interactions indirectly cause apoptosis within the cell.<sup>[20,23,24]</sup>

Consequently, these proteins have been the target of intense medicinal chemistry efforts towards the discovery of new treatments for cancer.<sup>[22,30–35]</sup> Although clinical trials are ongoing, to date there are no FDA-approved Mcl-1 or HDM2 inhibitors, with only one Bcl-2 selective inhibitor, venetoclax, that has reached the clinic.<sup>[36]</sup> However, studies have shown that venetoclax-treated cancer cells develop chemoresistance by overexpressing other anti-apoptotic proteins, most notably Mcl-1, re-affirming the unmet medical need of developing Mcl-1 inhibitors.<sup>[37,38]</sup>

In a phase II study evaluating venetoclax in patients with relapsed/refractory acute myeloid leukemia (AML), a 19% response rate was observed. 34% of patients in this study escalated to 1200 mg of venetoclax due to lack of response at the initial 800 mg dose, which did not achieve additional response.<sup>[39]</sup> Next, a phase Ib clinical trial was employed to assess a combination therapy of venetoclax and idasanutlin, an HDM2 inhibitor, in relapsed/refractory acute myeloid leukemia (AML) due to the modest monotherapy response rate. This combination was explored due to the overexpression of Mcl-1 in venetoclax-resistant cells, compounded with the knowledge that the inhibition of HDM2 and subsequent activation of p53 can result in Mcl-1 degradation. They reported 35.9% of patients responded to treatment. Of 39 patients treated, 14 exhibited antileukemic response which include complete and partial remission.<sup>[40]</sup> Currently, a phase I/II study is ongoing to determine the safety, tolerability, pharmacokinetics of the combination therapy in pediatric and young adult patients with relapsed/refractory acute leukemias or solid tumors (NCT04029688).

Additionally, a recent study involving the Mcl-1 selective inhibitor S63845 and the HDM2 inhibitor HDM201 evaluated the cell viability of combination treatments in AML cells.<sup>[41]</sup> MOLM-13 and OCI-AML-3 cells were susceptible to S63845 monotherapy with 60–70% viability, while OCI-AML-2 cells were 95% viable. In contrast, OCI-AML-2 AND MOLM-13 cells were susceptible to HDM201 monotherapy with 80% viability, whereas OCI-AML-3 showed no reduction. All three cell lines showed synergistic effects, with the combination index (CI)=0.2–0.5 when treated with both drugs, while OCI-AML-3 exhibited a strong synergy effect with CI=0.2–0.3.<sup>[41]</sup> These studies represent the efficacy of combination therapies of an anti-apoptotic protein inhibitor with an HDM2 inhibitor.

An alternative strategy to these polypharmacy regimens is polypharmacology, in which one drug is fashioned to recognize multiple targets. Polypharmacology is an emerging field of research and could provide multiple benefits to the patient, including increased patient compliance, eliminated drug-drug interactions, and reduced side effects, not only through a reduction in drug cocktail complexity but also broadened therapeutic windows through greater therapeutic efficacies with reduced doses.<sup>[42,43]</sup> In light of these studies, coupled with the multifactorial nature of cancer that suggests multiple drugs, or a single drug presenting multiple pharmacophores, will be required for an effective pharmacotherapy, we herein describe a polypharmacology approach to address the unmet need of Mcl-1 and HDM2 inhibitors in the clinic using synthetic  $\alpha$ -helix mimicry.

## Results and Discussion

Both the Bim-BH3 and p53TAD  $\alpha$ -helices project similar hydrophobic character at “hot spot” residues  $i$ ,  $i+3/4$ , and  $i+7$ : Leu62, Ile65, and Phe69 in Bim (Figure 1B), and Phe19, Trp23, and Leu26 in p53TAD (Figure 1D).<sup>[44–46]</sup> Importantly, there is a conserved arginine residue on pro-life proteins (Arg263 in Mcl-1) that forms a salt bridge with Asp67 on the Bim  $\alpha$ -helix at the  $i+5$  position.<sup>[47]</sup> Additionally, there is an aspartate residue in an analogous location ( $i+2$ ) in p53TAD (Asp21), that helps maintain the integrity of the helix rather than engage in recognition.<sup>[48]</sup> We set out to capitalize on these similarities across both  $\alpha$ -helices towards the discovery of dual inhibitors of Mcl-1 and HDM2.

Monocyclic scaffolds such as terphenyl, imidazoline, and pyrazole scaffolds have been used as scaffolds to effectively mimic either the BH3 or the p53  $\alpha$ -helices.<sup>[4,13,49]</sup> Roche introduced small molecules based on *cis*-imidazolines as inhibitors of HDM2, leading to the discovery of the nanomolar inhibitor Nutlin-3a.<sup>[50]</sup> As evidenced by a co-crystal structure of Nutlin-3a and HDM2, the isopropoxyphenyl group mimics Phe19, while the two 4-chlorophenyl groups projected in a *cis*-1,2-functionalization from the imidazoline scaffold mimic Trp23 and Leu26 (PDB ID: 4 J3E; Figure 2).<sup>[22]</sup>

Given Nutlin 3a's effective mimicry of the p53TAD helix, which resembles the Bim-BH3 helix, perhaps it is unsurprising that it also exhibits low micromolar inhibition of Bcl-2.<sup>[22]</sup> In

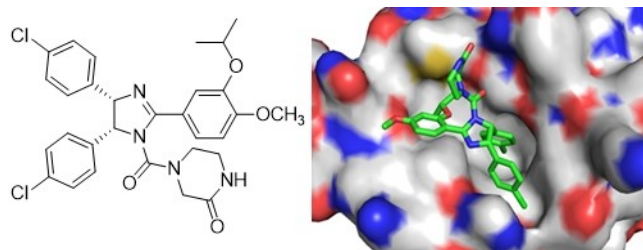


**Figure 2.** Nutlin 3a co-crystallized with HDM2 (PDB ID: 4 J3E).

patent CA2771936 A1, Novartis describe sub-nanomolar inhibitors of HDM2 based on tetra-substituted heteroaryl scaffolds

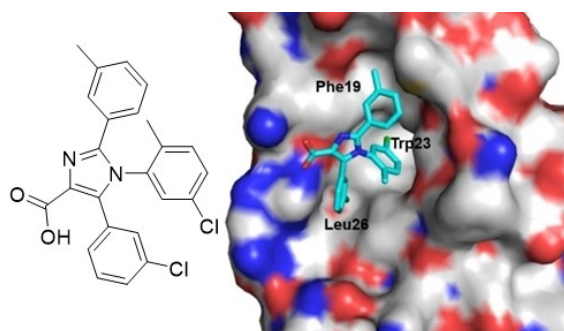


**Figure 3.** Co-crystal structure of Novartis compound and HDM2 (PDB ID: 4OQ3). Residue labels indicate the binding locations of the key residues in the p53TAD helix.

including imidazoles, pyrazoles, and pyrroles. The most potent compounds project aryl functional groups in a 1,2,3-substitution pattern, indicating a clustered projection appears optimal.<sup>[51]</sup> PDB ID 4OQ3 illustrates the co-crystal structure of one of these imidazole-based inhibitors with HDM2 (Figure 3). The three functional groups engage in multiple contacts with the protein with each functional group projected into the respective pockets: 3-chlorophenyl in a  $\pi$ - $\pi$  interaction with His96 while mimicking Leu26, 2-methyl, 5-chlorophenyl sitting in the Trp23 pocket, and the 3-methylphenyl functional group mimicking Phe19.<sup>[46]</sup> More recently, Zhang et al. developed a dual Bcl-2/HDM2 inhibitor based on a pyrazole scaffold (Figure 4, center structure). As shown in Figure 3, their work is very closely related to the corresponding pyrazoles from Novartis (Figure 4, left structure) with a noticeable departure being the incorporation of an amide group between the pyrazole core and one of the aryl side chains. The authors reasoned this flexible amide bond was incorporated to promote mimicry of the less-structured p53TAD  $\alpha$ -helix, while retaining effective mimicry of the BH3  $\alpha$ -helix. The most potent inhibitor of Bcl-2, Mcl-1, and HDM2 achieved affinities of  $K_i=0.140$ ,  $0.161$ , and  $0.107$   $\mu\text{M}$ , respectively.<sup>[45]</sup>

Leveraging the successes from Novartis and Zhang with heavily functionalized pyrazoles to inhibit the Bcl-2 family of proteins and HDM2, coupled with the effective deployment of the acyl sulfonamide functional group as a carboxylic acid bioisostere in Mcl-1 inhibitors elsewhere, we designed a library of three novel, densely functionalized scaffolds to mimic the BH3 binding domain and p53TAD: isoxazoles, pyrazoles, and thiazoles (Figure 4, right structure), which are all present in

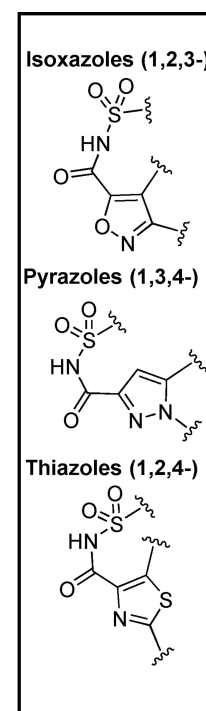
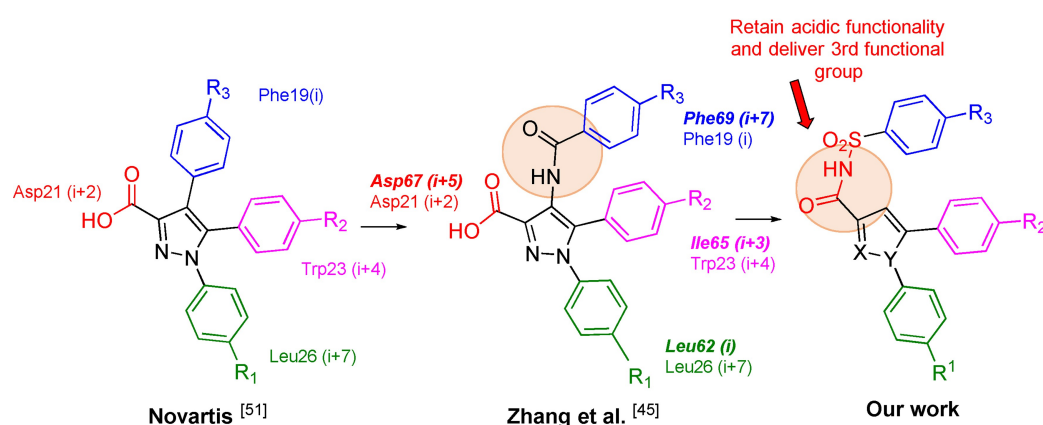


**Figure 4.** Representative structures of Novartis patent CA2771936 A1 (left), Zhang et al. Dual Bcl-2/HDM2 inhibitor (center), and our work presented in this manuscript (right). Normal font represents p53TAD residues; bold, italic font represents Bim-BH3 residues.

pharmacologically active drug molecules.<sup>[52–55]</sup> Each scaffold will allow us to explore the protein binding interfaces with different substitution patterns: isoxazoles represent a 1,2,3-functionalization (with the numbering starting with the acyl substituent), pyrazoles represent a 1,3,4-functionalization, and thiazoles a 1,2,4-functionalization. In addition to sustaining the acidity needed to engage Arg263 of Mcl-1, incorporation of the acyl sulfonamide functional group ( $pK_a$  5) – akin to the amide in Zhang's work – was hypothesized to ensure delivery of the third aryl group to both Mcl-1 and HDM2 by providing additional flexibility that permits effective mimicry of the more rigid BH3  $\alpha$ -helix and equally the less-structured p53  $\alpha$ -helix. Figure 5 shows the overlay of an energy-minimized conformation of acyl sulfonamide isoxazole **OX0** in which all R groups were fixed as isopropyl groups. Good mimicry of the key side chains (highlighted) of both helical peptides is suggested, which is expected to translate into potent inhibition of Mcl-1 and HDM2. Since the acyl sulfonamide portion is intended to emulate the carboxylic acid on one face of the helix as well as a hydrophobic group on the opposing face, while the R<sup>1</sup> and R<sup>2</sup> are intended to emulate adjacent hydrophobic groups on the same face of the helix, we hypothesize that the isoxazoles and pyrazoles will be more potent inhibitors than the corresponding thiazoles which carry an inferior substitution pattern.

### Computer-aided drug design

We employed computer-aided drug design (CADD) using SILCS, site identification by ligand competitive saturation, to assist in compound library design efforts.<sup>[56–58]</sup> Unlike other CADD methods, SILCS takes protein flexibility and desolvation into account. SILCS initially involves molecular dynamics (MD) simulations of the target protein in the presence of organic solutes immersed in an aqueous environment, which compete for binding sites on the protein. Analysis of the distribution of organic solutes yields 3D residence fragment probability distributions that are used to map functional group affinity patterns, termed FragMaps. These FragMaps include aliphatic, aromatic, hydrogen bond donors and acceptors, heterocycles and charged functional groups that are converted into grid free

energies (GFEs).<sup>[59]</sup> Visualization of the FragMaps allows for the identification of synthetically accessible specific functional groups that will maximize interactions with proteins. SILCS Monte-Carlo (SILCS MC) sampling can be used in conjunction with the FragMaps for ligand docking from which Ligand-GFE (LGFE) scores are obtained, providing a quantitative ranking of different ligands.<sup>[60]</sup> This aids in the design of functional group modifications on the inhibitors to increase affinity for the target protein. In the present study the SILCS approach is used simultaneously on Mcl-1 and HDM2 to identify functional groups that will maximize affinity for the two proteins in the context of a rational polypharmacology design approach.

Next, **OX0** was docked into Mcl-1 (Figure 6A) and HDM2 (Figure 6B) by using SILCS to show the binding mode of our compounds and determine their ability to occupy regions that are favorable for binding of the design functional groups. Figure 7 shows the SILCS-MC docked orientations of **OX0** in Mcl-1 (left) and HDM2 (right), along with FragMaps for aliphatic (green) and aromatic (purple) functional groups. This informs us where additional moieties should be grafted onto our inhibitors to ensure more favorable contacts with the proteins.<sup>[13]</sup> In both proteins, the hydrophobic functional groups projected from the core scaffold are encased almost entirely within the FragMaps

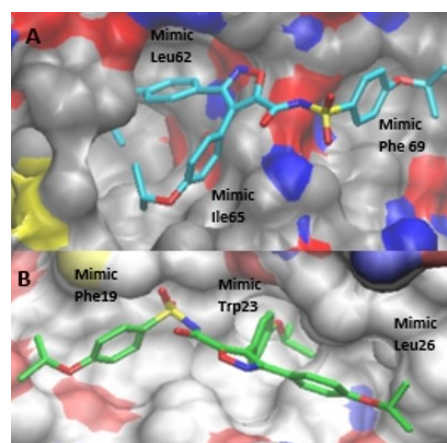


Figure 6. SILCS MC docking with **OX0** in A) Mcl-1 and B) HDM2.

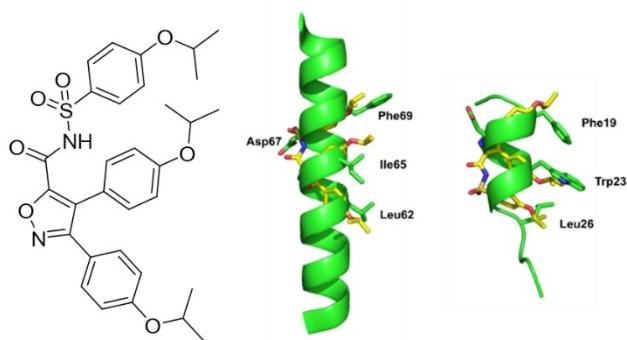


Figure 5. Energy minimization of **OX0** in ChemDraw3D and overlaid with Bim-BH3 (center) and p53TAD (right)  $\alpha$ -helices.

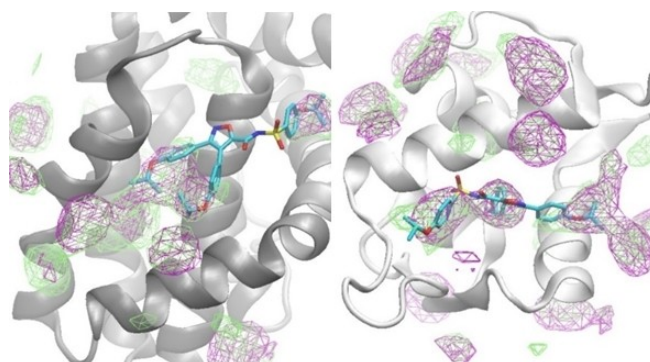
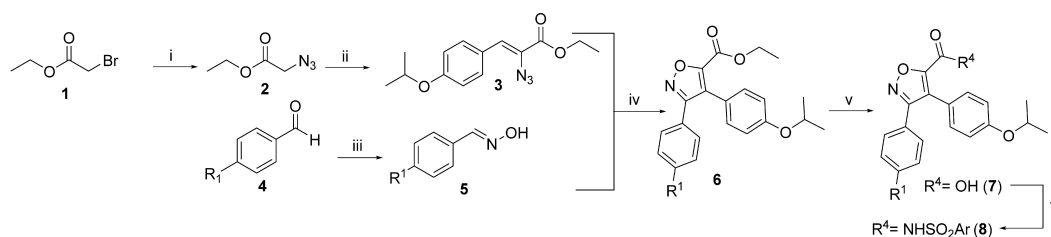
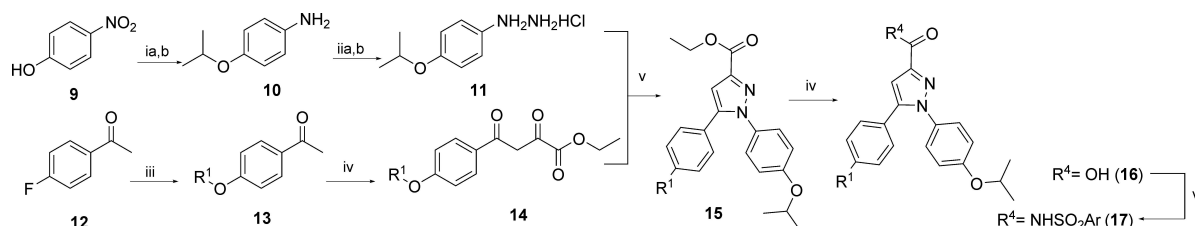


Figure 7. **OX0** docked in Mcl-1 (left) and HDM2 (right) with SILCS.



**Scheme 1.** i)  $\text{NaN}_3$ , DMF, RT, 18 h; ii) (4-OiPr)benzaldehyde, NaH, EtOH,  $-10^\circ\text{C}$ , 4 h; iii)  $\text{NH}_2\text{OH}\cdot\text{HCl}$ , pyridine, reflux, 1 h; iv)  $\text{Et}_3\text{N}$ , NCS, DMF, RT to  $90^\circ\text{C}$ , 18 h; v)  $\text{LiOH}\cdot\text{H}_2\text{O}$ , THF/MeOH/ $\text{H}_2\text{O}$ , RT, 18 h; vi) corresponding sulfonamide, isobutyl chloroformate, NMM, NaH, THF,  $-10^\circ\text{C}$  to  $0^\circ\text{C}$  to RT, 18 h.

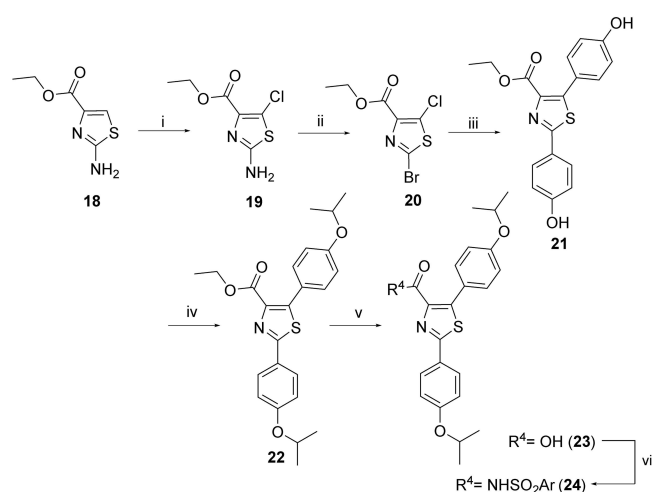


**Scheme 2.** i) a) 2-iodopropane,  $\text{K}_2\text{CO}_3$ , DMF, RT to  $60^\circ\text{C}$ , 18 h; b)  $\text{SnCl}_2\cdot 2\text{H}_2\text{O}$ , EtOAc,  $50^\circ\text{C}$ , 18 h; ii) a)  $\text{NaNO}_2$ ,  $\text{H}_2\text{O}$ ,  $0^\circ\text{C}$ , 18 h; ii) b)  $\text{SnCl}_2\cdot 2\text{H}_2\text{O}$ , EtOAc,  $50^\circ\text{C}$ , o/n; iii) corresponding alcohol,  $\text{K}_2\text{CO}_3$ , DMF,  $60^\circ\text{C}$ , 18 h; iv) diethyl oxalate, NaH, THF,  $0^\circ\text{C}$  to RT, 18 h; v) AcOH, reflux, 18 h; vi)  $\text{LiOH}\cdot\text{H}_2\text{O}$ , THF/MeOH/ $\text{H}_2\text{O}$ , RT, 18 h; vii) corresponding sulfonamide, isobutyl chloroformate, NMM, NaH, THF,  $-10^\circ\text{C}$  to  $0^\circ\text{C}$  to RT, 18 h.

indicating that they are in the correct orientation to mimic the native ligand and thereby improve the binding affinity.

## Synthesis

Target molecules based on the generic structures shown in Figure 4 (right), were accessed as depicted in Scheme 1–3. In order to evaluate our design strategy, the  $\text{R}^1$ ,  $\text{R}^2$  and  $\text{R}^3$  groups



**Scheme 3.** i) NCS, ACN,  $80^\circ\text{C}$ , 18 h; ii)  $\text{tBuONO}$ ,  $\text{CuBr}_2$ , ACN,  $80^\circ\text{C}$ , 18 h; iii) 4-hydroxyphenylboronic acid, CsF, tetrakis(triphenylphosphine)palladium(0), DME/MeOH,  $80^\circ\text{C}$ , 18 h; iv) 2-iodopropane,  $\text{K}_2\text{CO}_3$ , DMF,  $50^\circ\text{C}$ , 18 h; v)  $\text{LiOH}\cdot\text{H}_2\text{O}$ , THF/MeOH/ $\text{H}_2\text{O}$ , RT, 18 h; vi) corresponding sulfonamide, isobutyl chloroformate, NMM, NaH, THF,  $-10$  to  $0^\circ\text{C}$  to RT, 18 h.

were restricted to a focus set of hydrophobic side chains, including isopropyl and phenyl.

**Isoxazoles:** Azidation of ethylbromoacetate (1) followed by a Knoevenagel condensation with 4-isopropoxybenzaldehyde (2) delivered ethyl (Z)-2-azido-3-(4-isopropoxyphenyl)acrylate (3). Meanwhile, various 4-substituted benzaldehydes 4 were transformed into (E)-benzaldehyde oximes 5 under standard conditions. Subsequently, N-chlorosuccinimide mediated the cyclization of acrylates 3 with oximes 5 to construct the isoxazole scaffold in compounds 6. Saponification of the ethyl esters revealed the carboxylic acids 7, which were finally coupled with various sulfonamides to afford the 1,2,3-functionalized isoxazole acyl sulfonamides 8.

**Pyrazoles:** Isopropylation of 4-nitrophenol (9) followed by reduction with tin(II) chloride yielded 4-isopropoxyaniline (10), which was subsequently transformed into hydrazine 11. Meanwhile, 4-fluoroacetophenone (12) underwent  $\text{S}_\text{N}\text{Ar}$  reactions with isopropanol or phenol to furnish the 4-substituted phenol ethers 13, which underwent Claisen ester condensations with diethyl oxalate to deliver  $\beta$ -keto esters 14. In an application of the Knorr pyrazole synthesis, hydrazines 11 were condensed with  $\beta$ -keto esters to yield the 1,2,4-trisubstituted pyrazoles 15. Saponification as before delivered the corresponding carboxylic acids 16, which were subsequently coupled to the library of sulfonamides to furnish the 1,3,4-trisubstituted pyrazole acyl sulfonamides 17.

**Thiazoles:** Briefly, ethyl-2-aminothiazole-4-carboxylate (18) was chlorinated in the remaining aromatic position and then subjected to a Sandmeyer transformation to deliver the 2-bromo-5-chlorothiazole-2-carboxylate derivative 20. Both halogens were displaced in a double Suzuki reaction employing an excess of 4-hydroxybenzeneboronic acid, and then both

phenols were alkylated with isopropyl iodide to yield **22**. Saponification as before delivered the carboxylic acid **23**, and conjugation to our library of sulfonamides furnished the target molecules, 1,2,4-tri-substituted thiazole acyl sulfonamides **24**.

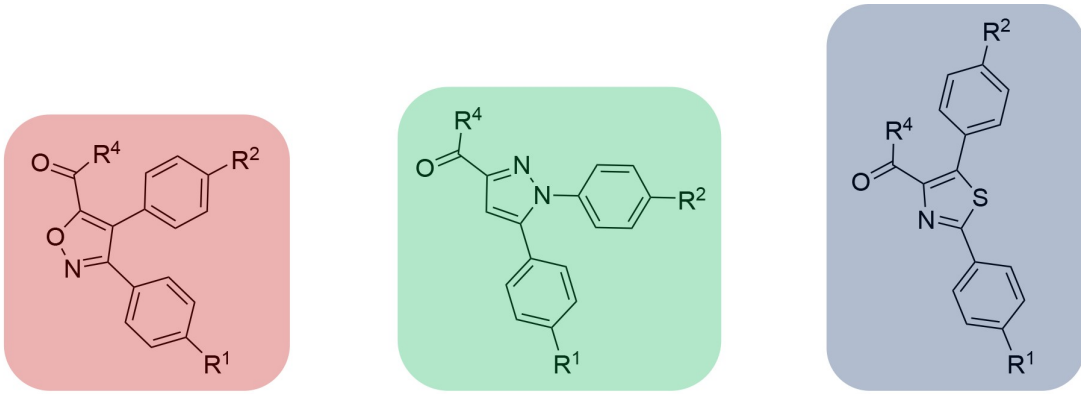
## Results

Binding affinities of target molecules to Mcl-1 and HDM2 were determined by a standard fluorescence anisotropy competition assay using FITC (fluorescein isothiocyanate)-labeled Bak-BH3 for Mcl-1 or TAMRA (tetramethylrhodamine)-labeled p53 for HDM2; these data are presented in Table 1. As we prepared a focused set of inhibitors, it would be premature at this stage to delve into a detailed discussion on R<sup>1</sup>, R<sup>2</sup> and R<sup>4</sup> side chains, and that will be reserved for a follow-up full paper with a larger library of compounds. However, it is clear that in every case,

compounds were more potent inhibitors of Mcl-1 than HDM2, ranging from around three-fold to >100-fold better. Furthermore, the isoxazoles and pyrazoles were, generally, the most potent dual inhibitors, and, likely owing to the inferior substitution pattern that was referred to earlier, the thiazoles were the worst inhibitors. Of course, we cannot rule out that the identity and location of the heteroatoms in each core did not impact binding affinity, as well, and this will be investigated at a later date. It is noteworthy that the more potent isoxazoles and pyrazoles have a more clustered projection of "side chains" similar to the potent HDM2 inhibitor Nutlin-3a, and a co-crystal structure of Nutlin-3a/HDM2 reveals the three sub-pockets on HDM2 are close together (PDB ID: 4J3E). This superior functionality is present in both the Novartis patent and the Zhang *et al.* dual inhibitor.<sup>[45,51]</sup>

We hypothesized that the conversion of the carboxylic acid to an acyl sulfonamide would offer greater inhibition, accom-

**Table 1.** Inhibition of Mcl-1 and HDM2 with isoxazoles, pyrazoles, and thiazoles using fluorescence anisotropy competition assay (FACA).



Compound Number	R <sup>1</sup>	R <sup>2</sup>	R <sup>4</sup>	Mcl-1	K <sub>i</sub> (μM)	HDM2
<b>7a</b>	-OiPr	-OiPr	-OH	11.4 ± 1.0	85.8 ± 16.2	
<b>7b</b>	-OPh	-OiPr	-OH	2.83 ± 0.30	18.6 ± 3.9	
<b>16a</b>	-OiPr	-OiPr	-OH	10.6 ± 0.7	84.4 ± 16.9	
<b>16b</b>	-OPh	-OiPr	-OH	3.12 ± 7	15.4 ± 2.9	
<b>23</b>	-OiPr	-OiPr	-OH	10.4 ± 0.8	27.9 ± 5.1	
<b>8a</b>	-OiPr	-OiPr	-NHSO <sub>2</sub> (4-OCF <sub>3</sub> )Ph	2.91 ± 0.11	41.5 ± 8.3	
<b>8b</b>	-OPh	-OiPr	-NHSO <sub>2</sub> (4-OCF <sub>3</sub> )Ph	0.263 ± 0.018	NA	
<b>8c</b>	-OPh	-OiPr	-NHSO <sub>2</sub> (4-OPh)Ph	0.355 ± 0.02	33.4 ± 4.2	
<b>8d</b>	-OPh	-OiPr	-NHSO <sub>2</sub> (2-naphthyl)	NA	NA	
<b>17a</b>	-OiPr	-OiPr	-NHSO <sub>2</sub> (4-OCF <sub>3</sub> )Ph	5.89 ± 0.03	41.0 ± 7.4	
<b>17b</b>	-OPh	-OiPr	-NHSO <sub>2</sub> (4-OPh)Ph	2.05 ± 1.62	16.5 ± 2.1	
<b>17c</b>	-OPh	-OiPr	-NHSO <sub>2</sub> (4-OCF <sub>3</sub> )Ph	0.433 ± 0.033	11.5 ± 1.7	
<b>17d</b>	-OPh	-OiPr	-NHSO <sub>2</sub> (2-naphthyl)	0.561 ± 0.072	39.2 ± 8.3	
<b>24a</b>	-OiPr	-OiPr	-NHSO <sub>2</sub> (4-OCF <sub>3</sub> )Ph	5.14 ± 0.59	141 ± 26	
<b>24b</b>	-OiPr	-OiPr	-NHSO <sub>2</sub> (4-OPh)Ph	30.9 ± 7.26	263 ± 54	
<b>24c</b>	-OiPr	-OiPr	-NHSO <sub>2</sub> (2-naphthyl)	19.1 ± 2.2	NA	

NA: no activity. Data are represented as the average of experiments performed in triplicate ± SD. IC<sub>50</sub> values were converted into K<sub>i</sub> values by using the Nikolovska-Coleska equation.<sup>[61]</sup>

plishing mimicry of the third hydrophobic side chain. While the poor activity of the thiazole acid **23** could not be rescued in this way, the data for the isoxazoles and pyrazoles proved this hypothesis true in almost every case with Mcl-1 and in some of the cases with HDM2. This can be seen, for example, by comparing acid **7a** ( $K_i=11.4\ \mu\text{M}$  (Mcl-1),  $85.8\ \mu\text{M}$  (HDM2)) with its corresponding acyl sulfonamide **8a** ( $K_i=2.91\ \mu\text{M}$  (Mcl-1),  $41.5\ \mu\text{M}$  (HDM2)), as well as acid **16a** ( $K_i=10.6\ \mu\text{M}$  (Mcl-1),  $84.4\ \mu\text{M}$  (HDM2)) with the analogous acyl sulfonamide **17a** ( $K_i=5.89\ \mu\text{M}$  (Mcl-1),  $41.0\ \mu\text{M}$  (HDM2)). We attribute this to a combination of the retention of an acidic functionality needed to engage with Arg263 of Mcl-1, but also the excellent delivery of the third functional group  $R^4$  that is seen to overlap with the FragMaps in OX0 (Figure 6) in the modeling studies with both proteins, indicating their contribution to improved affinity. It should be noted that although OX0 was not synthesized, it is very similar to **8a**, and the intention of the FragMaps was to suggest analogues based on the modeled compound, such as **8a**. Closer inspection of the data suggests that the strategy of converting a carboxylic acid into a structurally more elaborate acyl sulfonamide had a greater beneficial impact on Mcl-1 inhibition than on HDM2 inhibition, and in some cases – predominantly isoxazoles – this actually proved detrimental to HDM2 inhibition. Of all compounds tested, our most potent dual inhibitor was pyrazole **17b** with  $K_i$  values of 433 nM and  $11.5\ \mu\text{M}$  for Mcl-1 and HDM2, respectively. Inadvertently, we may have identified a new scaffold for the development of selective Mcl-1 inhibitors, since some of our isoxazoles were potent against Mcl-1 with limited or no activity against HDM2, for example **8b** with a  $K_i$  of 263 nM for Mcl-1 and inactive against HDM2.

One of the challenges with developing dual inhibitors – through the same recognition motif – of Mcl-1 and HDM2 by  $\alpha$ -helix mimicry is the size mismatch between analogous side chains. Particularly, the middle side chain of the region of Bim-BH3 that is being emulated is relatively small (Ile65), whereas the corresponding residue in p53TAD is much larger (Trp23), and the respective pockets that bind these side chains do not appear malleable from crystal structures. On the other hand, Fesik's group has demonstrated that the p2 pocket on Mcl-1 that binds Leu62 of Bim-BH3 is somewhat plastic, and can accommodate larger groups;<sup>[37]</sup> indeed, this appears to be a significant source of ligand affinity. Thus, for an effective dual inhibitor, a large  $R^1$  group is required for Mcl-1 inhibition, but a large  $R^2$  group is required for HDM2 inhibition. The isoxazole scaffold cannot effectively meet these criteria simultaneously. However, the pyrazole scaffold can because the  $R^1$  and  $R^2$  groups are interchangeable with respect to the third substituent at the acyl sulfonamide functionality through rotation about the pyrazole-acyl bond, and this may be one reason why, in general, the pyrazole acyl sulfonamides fared better as dual inhibitors than the corresponding isoxazole acyl sulfonamides. In other words, the large  $R^1$  phenyl group in the pyrazole series can serve as an effective mimic of Leu62 at the located at the periphery of the BH3  $\alpha$ -helix and bind the plastic p2 pocket of Mcl-1, yet, on the other hand through pyrazole-acyl bond rotation, is also able to mimic the Trp23 in the middle of the p53TAD  $\alpha$ -helix.

## Conclusion

The discovery of targeted anticancer agents is an intense field of research that is constantly being met with defeat due to the development of resistance. Polypharmacology represents a paradigm shift in the treatment of multi-factorial diseases, such as cancer. Recognizing that Mcl-1 and HDM2 are both upregulated in similar cancers and their anticancer activities are regulated by similarly functionalized  $\alpha$ -helical domains in their partner proteins, we hypothesized that suitably functionalized heterocycles could be designed to simultaneously inhibit both Mcl-1 and HDM2. In summary, we have demonstrated that acyl sulfonamides of triply substituted isoxazoles and pyrazoles are effective dual  $\alpha$ -helix mimetics of the Bim-BH3 and p53TAD domains, inhibiting Mcl-1 and HDM2, respectively. Although our data presently indicate that the isoxazoles might be better suited to the development of selective Mcl-1 inhibitors, further optimization of the pyrazole core may lead to more potent dual inhibitors. Particularly, since conversion of the pyrazole acids to their corresponding acyl sulfonamides was more impactful for Mcl-1 than HDM2, we intend to first optimize the pyrazole acid predominantly to HDM2, and then anticipate a greater improvement in Mcl-1 affinity upon converting the acids to acyl sulfonamides.

## Experimental Section

Complete protocols for both chemical syntheses and biological methods together with characterization data are presented in the Supporting Information.

## Conflict of Interest

A.D.M. Jr. is co-founder and Chief Scientific Officer of SilcsBio LLC.

## Acknowledgements

We thank the National Institutes of Health (T32GM066706), and the University of Maryland School of Pharmacy for financial support of this research.

**Keywords:** apoptosis · cancer · heterocycles · polypharmacology · protein–protein interactions

- [1] A. L. G. Janda, *Curr. Top. Med. Chem.* **2011**, *11*, 258–280.
- [2] L. Mabonga, A. P. Kappo, *Biophys. Rev. Lett.* **2019**, *11*, 559–581.
- [3] R. S. Akhtar, J. M. Ness, K. A. Roth, *Biochim. Biophys. Acta Mol. Cell Res.* **2004**, *1644*, 189–203.
- [4] J. Sassone, A. Maraschi, F. Sassone, V. Silani, A. Ciammola, *Cell Death Dis.* **2013**, *4*, 772–772.
- [5] D. S. Luciani, S. A. White, S. B. Widenmaier, V. V. Saran, F. Taghizadeh, X. Hu, M. F. Allard, J. D. Johnson, *Diabetes* **2013**, *62*, 170–182.
- [6] S. Fletcher, A. D. Hamilton, *Curr. Opin. Chem. Biol.* **2005**, *9*, 632–638.
- [7] M. E. Lanning, S. Fletcher, *Future Med. Chem.* **2013**, *5*, 2157–2174.

- [8] V. Azzarito, K. Long, N. S. Murphy, A. J. Wilson, *Nat. Chem.* **2013**, *5*, 161–173.
- [9] M. Arkin, *Curr. Opin. Chem. Biol.* **2005**, *9*, 317–324.
- [10] B. L. Lampson, M. S. Davids, *Curr Hematol Malig Rep* **2017**, *12*, 11–19.
- [11] V. Tisato, R. Voltan, A. Gonelli, P. Secchiero, G. Zauli, *J. Hematol. & Oncology* **2017**, *10*, 133.
- [12] “Phase I Study of MIK665, a) Mcl-1 Inhibitor, in Patients With Refractory or Relapsed Lymphoma or Multiple Myeloma”, <https://clinicaltrials.gov/ct2/show/NCT02992483>, **2020**.
- [13] “Study of Safety and Efficacy of HDM201 in Combination With LEE011 in Patients With Liposarcoma”, <https://clinicaltrials.gov/ct2/show/NCT02343172>.
- [14] M. E. Lanning, P. T. Wilder, H. Bailey, B. Drennen, M. Cavalier, L. Chen, J. L. Yap, M. Rajé, S. Fletcher, *Org. Biomol. Chem.* **2015**, *13*, 8642–8646.
- [15] A. M. Petros, E. T. Olejniczak, S. W. Fesik, *Biochim. Biophys. Acta* **2004**, *1644*, 83–94.
- [16] A. Barnard, K. Long, D. J. Yeo, J. A. Miles, V. Azzarito, G. M. Burslem, P. A. Prabhakaran, T. Edwards, A. J. Wilson, *Org. Biomol. Chem.* **2014**, *12*, 6794–6799.
- [17] P. E. Czabotar, G. Lessene, A. Strasser, J. M. Adams, *Nat. Rev. Mol. Cell Biol.* **2014**, *15*, 49–63.
- [18] K. H. Vousden, D. P. Lane, *Nat. Rev. Mol. Cell Biol.* **2007**, *8*, 275–283.
- [19] R. J. Youle, A. Strasser, *Nat. Rev. Mol. Cell Biol.* **2008**, *9*, 47–59.
- [20] C. M. Adams, S. Clark-Garvey, P. Porcu, C. M. Eischen, *Front. Oncol.* **2019**, *8*. DOI: 10.3389/fonc.2018.00636.
- [21] M. S. Lee, J. H. Ha, H. S. Yoon, C. K. Lee, S. W. Chi Biochemical, *Biophysical Research Communications* **2014**, *445*, 120–125.
- [22] B. Vu, P. Wovkulich, G. Pizzolato, A. Lovey, Q. Ding, N. Jiang, J.-J. Liu, C. Zhao, K. Glenn, Y. Wen, C. Tovar, K. Packman, L. Vassilev, B. Graves, *ACS Med. Chem. Lett.* **2013**, *4*, 466–469.
- [23] M. N. Saha, H. Jiang, H. Chang, *Cancer Biol. Ther.* **2010**, *10*, 567–578.
- [24] E. Toufektchan, F. Toledo, *Cancers (Basel)* **2018**, *10*, DOI: 10.3390/cancers10050135.
- [25] G. Teoh, M. Urashima, A. Ogata, D. Chauhan, J. A. DeCaprio, S. P. Treon, R. L. Schlossman, K. C. Anderson, *Blood* **1997**, *90*, 1982–1992.
- [26] K. Kojima, M. Konopleva, T. McQueen, S. O'Brien, W. Plunkett, M. Andreeff, *Blood* **2006**, *108*, 993–1000.
- [27] J. I.-J. Leu, P. Dumont, M. Hafey, M. E. Murphy, D. L. George, *Nat. Cell Biol.* **2004**, *6*, 443–450.
- [28] K. Kojima, T. McQueen, Y. Chen, R. Jacamo, M. Konopleva, N. Shinjima, E. Shpall, X. Huang, M. Andreeff, *Blood* **2011**, *118*, 4431–4439.
- [29] J. E. Chipuk, T. Kuwana, L. Bouchier-Hayes, N. M. Droin, D. D. Newmeyer, M. Schuler, D. R. Green, *Science* **2004**, *303*, 1010–1014.
- [30] S. Besbes, C. Billard, *Cell Death Dis.* **2015**, *6*, e1810.
- [31] A. Kotschy, Z. Szlavik, J. Murray, J. Davidson, A. L. Maragno, G. Le Toumelin-Braizat, M. Chanrion, G. L. Kelly, J.-N. Gong, D. M. Moujalled, A. Bruno, M. Csekei, A. Paczal, Z. B. Szabo, S. Sipos, G. Radics, A. Prosznyak, B. Balint, L. Ondi, G. Blasko, A. Robertson, A. Surgenor, P. Dokurno, I. Chen, N. Matassova, J. Smith, C. Pedder, C. Graham, A. Studeny, G. Lysiak-Auvity, A.-M. Girard, F. Gravé, D. Segal, C. D. Riffkin, G. Pomilio, L. C. A. Galbraith, B. J. Aubrey, M. S. Brennan, M. J. Herold, C. Chang, G. Guasconi, N. Cauquil, F. Melchior, N. Guigal-Stephan, B. Lockhart, F. Colland, J. A. Hickman, A. W. Roberts, D. C. S. Huang, A. H. Wei, A. Strasser, G. Lessene, O. Geneste, *Nature* **2016**, *538*, 477–482.
- [32] J.-C. Carry, C. Garcia-Echeverria, *Bioorg. Med. Chem. Lett.* **2013**, *23*, 2480–2485.
- [33] E. Whiting, M. R. Rajé, J. Chauhan, P. T. Wilder, D. Van Eker, S. J. Hughes, N. G. Bowen, G. E. A. Vickers, I. C. Fenimore, S. Fletcher, *Bioorg. Med. Chem. Lett.* **2018**, *28*, 523–528; I. L. Conlon, D. Van Eker, S. Abdelmalak, W. A. Murphy, H. Bashir, M. Sun, J. Chauhan, K. M. Varney, R. Godoy-Ruiz, P. T. Wilder, S. Fletcher, *Bioorg. Med. Chem. Lett.* **2018**, *28*, 1949–1953; M. E. Lanning, W. Yu, J. L. Yap, J. Chauhan, L. Chen, E. Whiting, L. S. Pidugu, T. Atkinson, H. Bailey, W. Li, B. M. Roth, L. Hynicka, K. Chesko, E. A. Toth, P. Shapiro, A. D. MacKerell Jr, P. T. Wilder, S. Fletcher, *Eur. J. Med. Chem.* **2016**, *113*, 273–292; B. Drennen, J. A. Scheenstra, J. L. Yap, L. Chen, M. E. Lanning, B. M. Roth, P. T. Wilder, S. Fletcher, *ChemMedChem* **2016**, *11*, 827–833; M. E. Lanning, P. T. Wilder, H. Bailey, B. Drennen, M. Cavalier, L. Chen, J. L. Yap, M. Rajé, S. Fletcher, *Org. Biomol. Chem.* **2015**, *13*, 8642–8646.
- [34] J. L. Yap, L. Chen, M. E. Lanning, S. Fletcher, *J. Med. Chem.* **2017**, *60*, 821–838; S. Fletcher, *Expert Opin. Ther. Pat.* **2019**, *29*, 909–919.
- [35] A. Beloglazkina, N. Zyk, A. Majouga, E. Beloglazkina, *Molecules* **2020**, *25*, 12.
- [36] “AbbVie Announces US FDA Approval of Venclexta (venetoclax) as a Chemotherapy-Free Combination Regimen for Previously Untreated Chronic Lymphocytic Leukemia Patients”, <https://www.drugs.com/new-drugs/abbvie-announces-us-fda-approval-venetoclax-venetoclax-chemotherapy-free-combination-regimen-4974.html>.
- [37] A. Friberg, D. Vigil, B. Zhao, R. N. Daniels, J. P. Burke, P. M. Garcia-Barrantes, D. Camper, B. A. Chauder, T. Lee, E. T. Olejniczak, S. W. Fesik, *J. Med. Chem.* **2013**, *56*, 15–30.
- [38] E. A. Punnoose, J. D. Levenson, F. Peale, E. R. Boghaert, L. D. Belmont, N. Tan, A. Young, M. Mitten, E. Ingalla, W. C. Darbonne, A. Oleksijew, P. Tapang, P. Yue, J. Oeh, L. Lee, S. Maiga, W. J. Fairbrother, M. Amiot, A. J. Souers, D. Sampath, *Mol. Cancer Ther.* **2016**, *15*, 1132–1144.
- [39] M. Konopleva, D. A. Pollyea, J. Potluri, B. Chyla, L. Hogdal, T. Busman, E. McKeegan, A. H. Salem, M. Zhu, J. L. Ricker, W. Blum, C. D. DiNardo, T. Kadia, M. Dunbar, R. Kirby, N. Falotico, J. Levenson, R. Humerickhouse, M. Mabry, R. Stone, H. Kantarjian, A. Letai, *Cancer Discov* **2016**, *6*, 1106–1117.
- [40] C. Caruso, *Cancer Discov* **2019**, *9*, 156.
- [41] K. Seipel, K. Schmitter, U. Bacher, T. Pabst, *Cancers (Basel)* **2019**, *11*, 1779.
- [42] A. S. Reddy, S. Zhang, *Expert Rev Clin Pharmacol* **2013**, *6*, 41–47.
- [43] A. Anighoro, J. Bajorath, G. Rastelli, *J. Med. Chem.* **2014**, *57*, 7874–7887.
- [44] G. J. P. Rautureau, M. Yabal, H. Yang, D. C. S. Huang, M. Kvensakul, M. G. Hinds, *Cell Death Dis.* **2012**, *3*, e443.
- [45] Z. Wang, T. Song, Y. Feng, Z. Guo, Y. Fan, W. Xu, L. Liu, A. Wang, Z. Zhang, *J. Med. Chem.* **2016**, *59*, 3152–3162.
- [46] A. Vaupel, G. Bold, A. De Pover, T. Stachyra-Valat, J. Hergovich Lisztwan, J. Kallen, K. Masuya, *Furet. Bioorganic & Medicinal Chemistry Letters* **2014**, *24*, 2110–2114; *Medicinal Chemistry Letters* **2014**, *24*, 2110–2114.
- [47] A. S. A. Mady, C. Liao, N. Bajwa, K. J. Kump, F. A. Abulwerdi, K. L. Lev, L. Miao, S. M. Grigsby, A. Perdihi, J. A. Stuckey, Y. Du, H. Fu, Z. Nikolovska-Coleska, *Sci. Rep.* **2018**, *8*, 10210.
- [48] C. Li, M. Pazgier, C. Li, W. Yuan, M. Liu, G. Wei, W.-Y. Lu, W. Lu, *J. Mol. Biol.* **2010**, *398*, 200–213.
- [49] H. Yin, G.-I. Lee, K. A. Sedey, O. Kutzki, H. S. Park, B. P. Orner, J. T. Ernst, H.-G. Wang, S. M. Sebt, A. D. Hamilton, *J. Am. Chem. Soc.* **2005**, *127*, 10191–10196.
- [50] L. T. Vassilev, B. T. Vu, B. Graves, D. Carvajal, F. Podlaski, Z. Filipovic, N. Kong, U. Kammlott, C. Lukacs, C. Klein, N. Fotouhi, E. A. Liu, *Science* **2004**, *303*, 844–848.
- [51] G. Bold, P. Furet, F. Gessier, J. Kallen, J. H. Lisztwan, K. Masuya, A. Vaupel, CA2771936A1, March 3, 2011.
- [52] N. F. Pelz, Z. Bian, B. Zhao, S. Shaw, J. C. Tarr, J. Belmar, C. Gregg, D. V. Camper, C. M. Goodwin, A. L. Arnold, J. L. Sensintaffar, A. Friberg, O. W. Rossanese, T. Lee, E. T. Olejniczak, S. W. Fesik, *J. Med. Chem.* **2016**, *59*, 2054–2066.
- [53] K. Kapadiya, K. Kavadia, P. Manvar, R. Kotadiya, R. Kothari, K. Ranjan, *Chemistry & Biology Interface* **2015**, *5*, 258–266.
- [54] D. K. Miyamoto, H. A. Flaxman, H.-Y. Wu, J. Gao, C. M. Woo, *ACS Chem. Biol.* **2019**, *14*, 2527–2532.
- [55] J. K. Gierse, Y. Zhang, W. F. Hood, M. C. Walker, J. S. Trigg, T. J. Maziasz, C. M. Koboldt, J. L. Muhammad, B. S. Zweifel, J. L. Masferrer, P. C. Isakson, K. Seibert, *J. Pharmacol. Exp. Ther.* **2005**, *312*, 1206–1212.
- [56] O. Guvench Jr., A. D. MacKerell, *PLoS Comput. Biol.* **2009**, *5*. DOI: 10.1371/journal.pcbi.1000435.
- [57] E. P. Raman, W. Yu, S. K. Lakkaraju, A. D. MacKerell, *J. Chem. Inf. Model.* **2013**, *53*, 3384–3398.
- [58] V. D. Ustach, S. K. Lakkaraju, S. Jo, W. Yu, W. Jiang, A. D. MacKerell, *J. Chem. Inf. Model.* **2019**, *59*, 3018–3035.
- [59] E. P. Raman, W. Yu, O. Guvench, A. D. MacKerell, *J. Chem. Inf. Model.* **2011**, *51*, 877–896.
- [60] M. Small, A. D. MacKerell in *In Silico Drug Discovery and Design: Theory, Methods, Challenges, and Applications*. (Ed.: C. Cavasotto), CRC Press, **2015**, 45–78.
- [61] Z. Nikolovska-Coleska, R. Wang, X. Fang, H. Pan, Y. Tomita, P. Li, P. P. Roller, K. Krajewski, N. G. Saito, J. A. Stuckey, S. Wang, *Anal. Biochem.* **2004**, *332*, 261–273..

Manuscript received: April 27, 2020

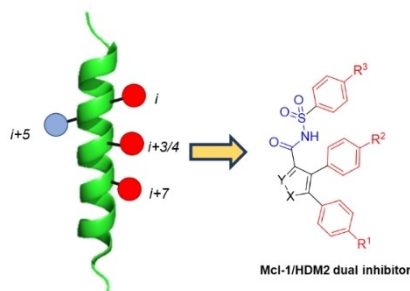
Revised manuscript received: May 19, 2020

Version of record online: ■■■, ■■■■

## COMMUNICATIONS

---

The anti-apoptotic protein Mcl-1 and E3 ubiquitin ligase HDM2 are both frequently upregulated in cancer. A small-molecule inhibitor can be developed by mimicking their protein binding partners, Bim and p53, to restore apoptosis in oncogenic cells. Through a polypharmacology approach, we have developed small-molecule  $\alpha$ -helix mimetics with isoxazole, pyrazole, and thiazole scaffolds that function as dual inhibitors of Mcl-1 and HDM2.



*I. L. Conlon, Dr. B. Drennen, Dr. M. E. Lanning, S. Hughes, R. Rothhaas, Dr. P. T. Wilder, Dr. A. D. Mackerell, Jr., Dr. S. Fletcher\**

1 – 9

**Rationally Designed Polypharmacology:  $\alpha$ -Helix Mimetics as Dual Inhibitors of the Oncoproteins Mcl-1 and HDM2**

